HEFAT2014
10th International Conference on Heat Transfer, Fluid Mechanics and Thermodynamics
14 – 16 July 2014
Orlando, Florida

CONTACT LINE FRICTION ANALYSIS OF WATER DROPLETS ON MICRO\NANOSCALE ROUGH STRUCTURES

Nima Sadeghpour, Sara Nahang Toudeshki, and Jiangtao Cheng*
*Author for correspondence
Department of Mechanical and Energy Engineering,

University of North Texas,

Texas, Denton, 76207

United States of America,

E-mail: Jiangtao.Cheng@unt.edu

ABSTRACT

In this paper we report the effects of surface roughness on contact line friction coefficients of water droplets on micro- and nano-patterned surfaces. Both advancing and receding contact line friction coefficients have been measured, analyzed and compared on smooth, one-tier (with micropillars), and two-tier (with carbon nanotubes (CNTs) grown on micropillars) surfaces over a wide range of contact line velocities and droplet volumes. Our results indicate that superhydrophobic surfaces with CNTs on top of micropillars can significantly decrease both the advancing and receding contact line friction coefficients. In comparison, both the advancing and receding contact line friction coefficients on smooth surfaces were more than ten times larger than those on superhydrophobic surfaces. However, droplets on one-tier surfaces with only micropillars exhibit different dynamic behaviors on advancing and receding movements. We experimentally investigated the Wenzel-Cassie transition on micropillar structures and found that the receding motion on micropillars is dominated by the Wenzel behavior, which leads to higher receding contact line friction coefficients on one-tier surfaces. However, there is a high tendency for an advancing droplet to exhibit Cassie-type behaviors on one-tier surfaces. As a result, advancing contact line friction coefficient is considerably mitigated on micropillars. On two-tier superhydrophobic surfaces, it was the Cassie–Baxter behavior that dominates both the advancing and receding contact line motions giving rise to less friction coefficients. Furthermore, the effects of surface roughness on contact line hysteresis are discussed in this paper.

INTRODUCTION

Superhydrophobic surfaces have unique properties such as large liquid contact angle (>150°), low contact angle hysteresis (<5°) and strong water repellence, which have been the subject of numerous studies over past decades [1-4]. In nature, some plants such as lotus leaves exhibit a large contact angle due to the intrinsic multiscale hierarchical micro\nano-structures on the surfaces. Indeed, introducing microscale roughness on to a smooth hydrophobic surface can give rise to significantly enhanced hydrophobicity, i.e., superhydrophobicity [5,6]. Some studies have investigated the influence of roughness geometry on wetting properties of superhydrophobic surfaces [7,8] and found that the geometry of microstructures (post size, height and spacing) plays important roles in the wetting mode of a textured surface. Owing to their unique properties superhydrophobic surfaces have significant potentials for practical applications. Recent studies have observed continuous dropwise condensation of water vapor on biomimetic lotus-leaf-like surfaces that could result in higher heat transfer coefficients [9,10]. Therefore, it is imperative to understand liquid dynamics (e.g., dynamic growth of dropwise condensate, contact line friction, et al.) on multiscale textured surfaces.

Previously, Voue et al. analyzed the effect of alkyl chain length on contact line friction coefficient of liquid droplets on self-assembled monolayers [11]. In this work, we aim to

measure and analyze the contact line friction coefficients of water droplets on smooth, one-tier (with micropillars), and two-tier (with carbon nanotubes (CNTs) grown on micropillars) surfaces. Our main objective is to investigate the influence of surface roughness on the contact line friction coefficient, which is defined by the following relation [12]:

$$\xi = \frac{\gamma\left|\cos\theta_s - \cos\theta_d\right|}{U_c} \qquad (1)$$

where ξ is the contact line friction coefficient, U_c is the contact line velocity, γ is the surface tension, θ_s is the static contact angle, and θ_d is the dynamic contact angle. This formula is derived directly from the molecular kinetic theory (MKT) [13,14]. According to this relation, determination of the contact line friction coefficient relies on precise measurements of the static and dynamic contact angles. Higher differences between static and dynamic contact angles lead to a greater contact line friction coefficient; and a lower friction coefficient results from smaller differences between the static and dynamic contact angles. It is noteworthy that the contact line friction coefficient may have different values on the advancing and receding contact lines. Therefore, we need to monitor the dynamic movements of both the advancing and receding contact lines on each surface. Utilizing a high speed CCD camera (Phantom Miro M310) with a frame rate up to 3200 frames/s, we have accurately measured the advancing and receding contact angles in both static and dynamic states. Equation 1 indicates that the contact line friction coefficient ξ is inversely proportional to the contact line velocity U_c. The frames are also used to calculate the advancing and receding contact line velocities. In order to investigate the influence of contact line velocity on the contact line friction coefficient, we have conducted our measurements with various velocities of water droplets. The term $|cos\theta_s - cos\theta_d|$ in eq. 1 indicates that in this work we only consider the absolute value of the difference between $cos\theta_s$ and $cos\theta_d$ and therefore we have the same sign for the advancing and receding contact line friction coefficients in our analysis.

In this study we investigated the effects of surface roughness on the advancing and receding contact line friction coefficients on smooth, one-tier, and two-tier surfaces as shown in Figure 1. The one-tier surface only consists of micropillars but two-tier superhydrophobic surfaces are artificially fabricated by integrating multiscale structures on a smooth substrate. First, square micropillars were formed on a silicon substrate by deep reactive ion etching (DRIE). A thin catalyst layer of nickel was subsequently deposited on the etched Si micropillars via e-beam evaporation. Then carbon nanotubes (CNTs) were grown on top of the micropillars by plasma enhanced chemical vapor deposition (PECVD). Coating with low-surface-energy materials is a widely used method to create hydrophobic properties [15,16].Therefore, in order to generate hydrophobic or superhydrophobic surfaces, a thin layer of fluoropolymer PFC1601V (Cytonix) was conformally coated on all samples leading to the apparent contact angles > 90°.

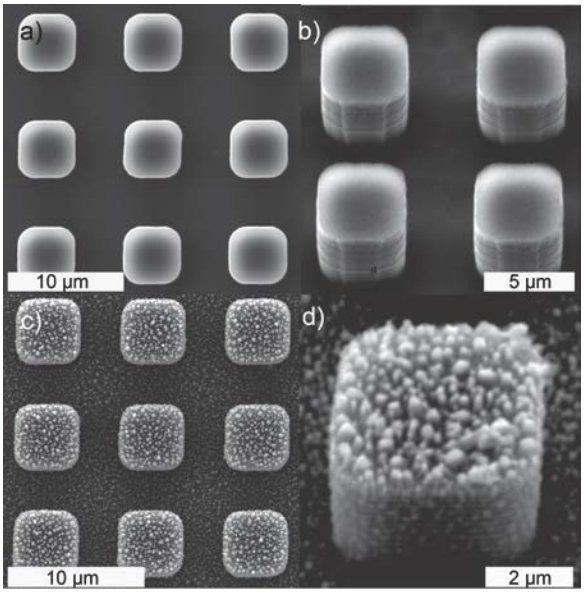

Figure 1 One-tier (a, b) and two-tier (c, d) structures. Images are captured by SEM. A thin layer of fluoropolymer is coated on the samples to make the intrinsic surfaces hydrophobic.

The wettability of a rough surface can be assessed by two different models suggested by Wenzel [17] and Cassie–Baxter [18]. According to the Wenzel model, water fills up the cavities on a rough surface and consequently droplets at the Wenzel state are highly pinned to the surface. In contrast, the Cassie–Baxter model assumes that the droplet stays on the top of the micro-structures of a rough surface with air trapped between these microtextures, which lead to a lower contact angle hysteresis and even automatic removal of a liquid droplet (so-called Lotus effect). Therefore, a rough surface seems stickier with droplets in the Wenzel State and seems more slippery with Cassie–Baxter-type droplets [19,20]. Both the Wenzel and Cassie models relate the apparent contact angles on a rough surface to the surface roughness geometry and the corresponding contact angle on the smooth surface:

Wenzel: $$\cos\theta_W = r\cos\theta_0 \qquad (2)$$

Cassie–Baxter: $$\cos\theta_{CB} = f(\cos\theta_0 + 1) - 1 \qquad (3)$$

where θ_w and θ_{CB} are the apparent contact angles on a rough surface corresponding to the Wenzel and Cassie–Baxter states, respectively. θ_0 is the Young's contact angle on a

smooth surface. r is the surface roughness factor and f is the fractional area of the wetted solid surface. For two-tier samples with nanotextures (with r_n and f_n) on top of microtextures (with r_m and f_m), the surface roughness ($r_m r_n$) is significantly augmented and the fraction of solid-liquid contact area $f_m f_n$ is remarkably reduced. In this work, we applied the Wenzel and Cassie–Baxter theories to analyze the effect of surface roughness on the contact line friction coefficients on both the one-tier and two-tier surfaces.

EXPERIMENTAL SETUP

Figure 2 shows the schematic of the experimental set up. First, a water droplet is placed on a hydrophobic substrate which is attached to a motorized translation stage (MTS50/M-Z8, Thorlabs). This substrate is coated with a thin layer of fluoropolymer (PFC1601V, Cytonix) everywhere on its surface except for a tiny area of 0.5mm x 0.5mm under the center of the droplet. The hydrophilic properties of this tiny area make the droplet stick to the substrate and move along with the translation stage. It is noteworthy that the entire shape of the droplet is not affected by this tiny hydrophilic area underneath and the droplet still exhibits a contact angle of ~123° on the substrate.

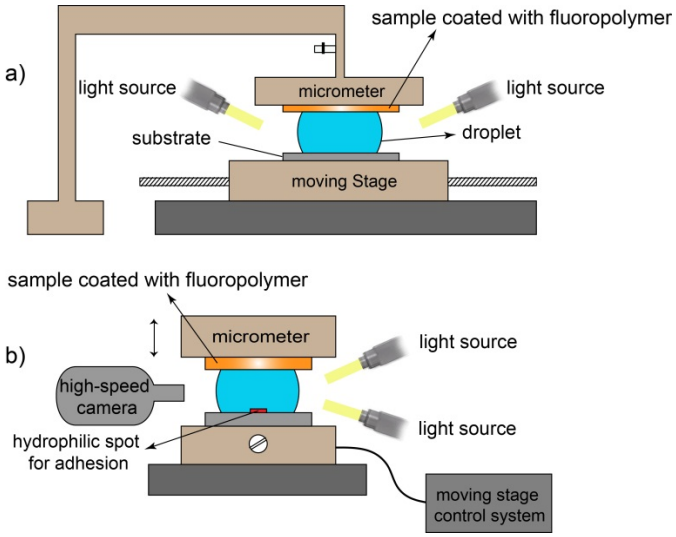

Figure 2 Schematic view of the experimental set up: a) front view, b) side view.

The velocity of the translation stage can be precisely controlled by its control system. In our experiments, the following stage velocities are used: 0.25, 0.5, 0.75, 1, 1.5, 2, 2.5 and 3 mm/s. Samples (smooth, or one-tier, or two-tier) are attached to a micrometer z-stage (NT66-495, Edmund Optics) above the droplet via a double-sided tape. Then we gradually lowered the sample until it slightly touched the droplet surface. In order to capture high-quality images, the droplet is properly sandwiched between the sample and the substrate. Two light beams (Dolan-Jenner MI-150 fiber optic illuminator) are adjusted behind the droplet for enhanced illumination. In this experimental configuration, the top surface of the droplet slides on the sample while its base is adhered to the translation stage. Gravity effect can be neglected in our analysis provided that the droplet is smaller than its capillary length ($l_{CA} = \sqrt{\frac{\gamma}{\rho g}}$); the capillary length of water is 2.7 mm). Figure 3 shows the schematics of a droplet transport on smooth, one-tier, and two-tier surfaces.

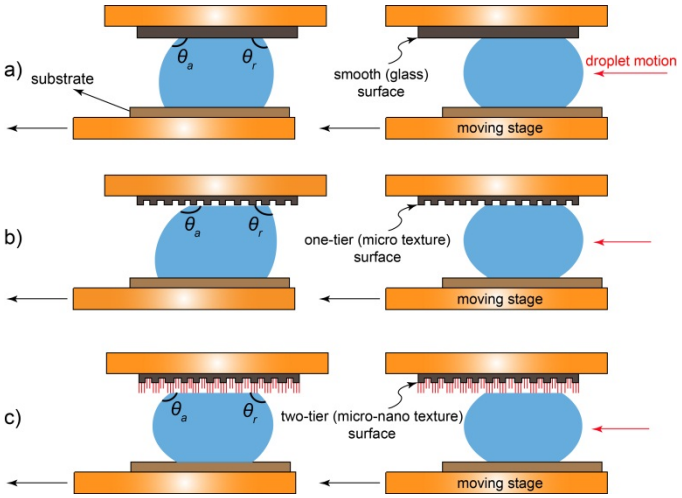

Figure 3 Schematic transport of a water droplet on: a) smooth, b) one-tier, and c) two-tier surfaces. All samples are coated with a thin layer of fluoropolymer.

Initially, the droplet is symmetric in shape having equal static contact angles on both sides. During movement, contact angle hysteresis makes the shape of the droplet asymmetric and the advancing contact angle becomes greater than the receding contact angle. As illustrated in Figure 3, on one-tier samples the receding contact angle differs from the static contact angle as high as ~30°; in contrast, the advancing contact angle changes slightly (2° to 4°), which is considerably smaller than the corresponding change on smooth samples. According to our measurements on two-tier samples, the advancing and receding contact angles differ about 0.5° to 2.5° from their static values. Therefore, extremely low advancing and receding contact line friction coefficients are expected on two-tier samples.

CONTACT LINE FRICTION COEFFICIENT ANALYSIS

Figure 4 plots the advancing and receding contact line friction coefficients of a water droplet of 25 μl versus the advancing and receding contact line velocities, respectively,

on smooth, one-tier, and two-tier surfaces. At relatively lower contact line velocities, it was observed that the contact line friction coefficient decreases with increasing droplet speed (and hence contact line velocity). But the friction coefficient reaches an approximately constant value at higher contact line velocities. In this study, this saturated value is considered as the contact line friction coefficient. As shown in Figure 4a, advancing contact line friction coefficients on different surfaces have the following relationship:

$$\xi_{adv-smooth} > \xi_{adv-one-tier} > \xi_{adv-two-tier}$$

In the advancing case, it seems that a higher surface roughness and a smaller solid fraction factor lead to a lower contact line friction coefficient.

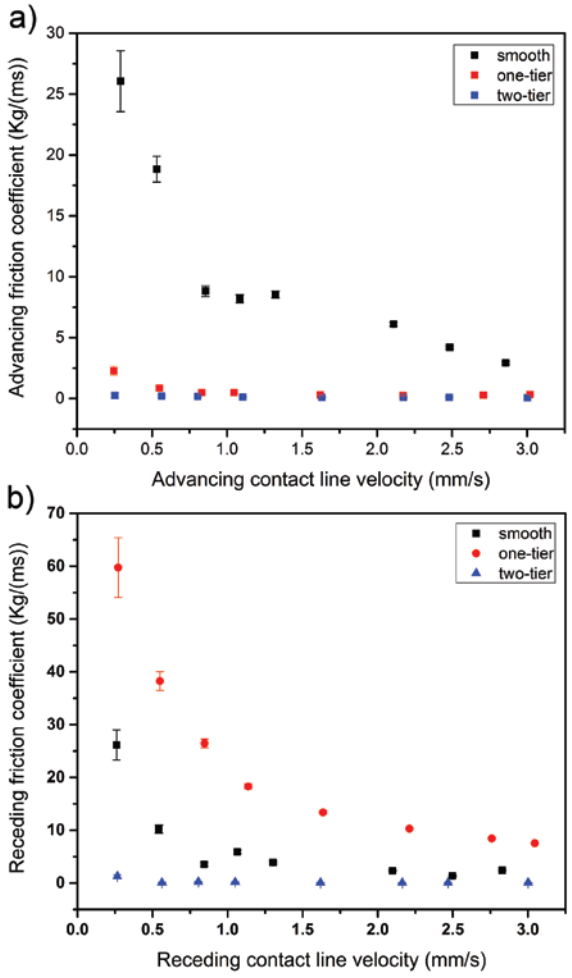

Figure 4 a) Comparison of the advancing contact line friction coefficients on different surfaces. b) Comparison of the receding contact line friction coefficients on different surfaces. The droplet volume in both diagrams is 25 µl.

The surface roughness of the one-tier sample (r_m) is lower than the surface roughness of the two-tier surface ($r_m r_n$) but larger than the smooth surface. Hence, the advancing contact line friction coefficients on the one-tier surface are larger than the corresponding values of the two-tier surface but are smaller than those values of the smooth surface.

Figure 4b compares the receding contact line friction coefficients on three surfaces. The friction coefficients on the receding event are found to follow:

$$\xi_{rec-one-tier} > \xi_{rec-smooth} > \xi_{rec-two-tier}$$

The receding contact line friction coefficients on the smooth surface are larger than the corresponding values of the two-tier surface but are smaller than the coefficients of the one-tier surface. Unlike the advancing case, the receding contact line friction coefficient on the one-tier surface has the highest value. This is due to the significant changes in the receding contact angle on the one-tier surface. Our experiments on the one-tier surface show that the difference between the static and dynamic contact angles on the advancing case is considerably low (about 2° to 4°), but the corresponding difference for the receding case is 25° to 40°. As a result, the one-tier surface has the highest receding contact line friction coefficient.

Our measurements indicate that the two-tier surface has the lowest friction coefficients on both the advancing and receding cases, which result from the extremely low difference between the static and dynamic contact angles.

DISCUSSION

According to our measurements, the receding contact line on the one-tier surface becomes sticky. Figure 5 illustrates the advancing and receding contact angle evolution while the droplet slid on the one-tier surface.

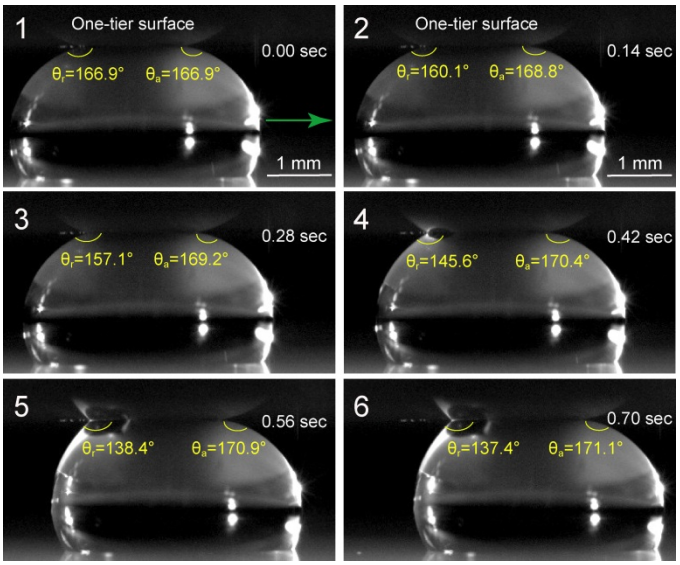

Figure 5 Snapshots of the receding contact angle change over time on the one-tier surface (top substrate). The droplet of **15 μl** moved leftward and the bottom stage velocity was **3** mm/s.

The bottom stage velocity was fixed at 3 mm/s and the droplet of 15 μl moved leftward. As can be seen in Figure 5, there was only a slight variation of about 2° to 4° in the advancing contact angle on the one-tier surface during droplet transport. In contrast, a marked change of the receding contact angle was observed. The receding contact angle differed from the static contact angle as much as 25° to 40° that resulted in a high dynamic contact angle hysteresis of 30° to 50°. As a consequence, the high contact angle hysteresis gave rise to a larger receding contact line friction coefficient. In the following discussion, we justify the considerable contact angle hysteresis on the one-tier surface.

Wettability of a rough surface can be analyzed by the Wenzel and Cassie–Baxter theories. For the one-tier surface as shown Figure 1, we have the following relations for r_m and f_m:

$$r_m = 1 + \frac{4a_m h_m}{p_m^2} \tag{4}$$

$$f_m = \frac{a_m^2}{p_m^2} \tag{5}$$

where a_m, h_m, and p_m are the width, height and pitch of the square micropillars, respectively. Therefore, eqs 2 and 3 can be rewritten as:

$$\text{Wenzel:} \quad \cos\theta_W = (1 + \frac{4a_m h_m}{p_m^2})\cos\theta_0 \tag{6}$$

$$\text{Cassie–Baxter:} \quad \cos\theta_{CB} = \frac{a_m^2}{p_m^2}(\cos\theta_0 + 1) - 1 \tag{7}$$

The geometric characteristics of the micropillars play a crucial role in the wetting behavior of a liquid and there exists a critical configuration (transition point) which demarcates the Wenzel and Cassie–Baxter regimes. In order to investigate the transition between these two regimes, a parameter called spacing factor s_f is defined as below [21]:

$$s_f = \frac{a_m}{p_m} \tag{8}$$

The one-tier sample with square micropillars has a specific ratio of $\frac{h_m}{a_m} = 0.95$ and the Wenzel and Cassie–Baxter relations can be rewritten as functions of the spacing factor s_f:

$$\text{Wenzel:} \quad \cos\theta_W = (1 + 3.8s_f^2)\cos\theta_0 \tag{9}$$

$$\text{Cassie–Baxter:} \quad \cos\theta_{CB} = s_f^2(\cos\theta_0 + 1) - 1 \tag{10}$$

where θ_0 is the liquid contact angle on a nominally smooth surface. The above equations can be extended in order to study the dynamic (advancing and receding) movements of liquids on a rough surface. We use $\theta_{0,adv}$ and $\theta_{0,rec}$ to stand for the advancing contact angle and the receding contact angle on the smooth surface, respectively. According to our measurements, $\theta_{0,adv} = 135°$ and $\theta_{0,rec} = 110°$ on our smooth hydrophobic sample. Thus, the advancing and receding contact line movements have different Wenzel-Cassie transition points. In order to investigate the transitions between the Wenzel and Cassie–Baxter states, we plot $\cos\theta$ versus s_f^2 for both the advancing and receding events (eqs. 9 and 10). Figure 6 illustrates the liquid state (Wenzel and Cassie) evolution in the advancing event with $\theta_{0,adv} = 135°$ and the advancing Cassie-Wenzel transition occurs at $s_f^2 = 0.098$. The black square in Figure 6 indicates our experimental value in the advancing case on the one-tier sample with $s_f^2 = 0.3$.

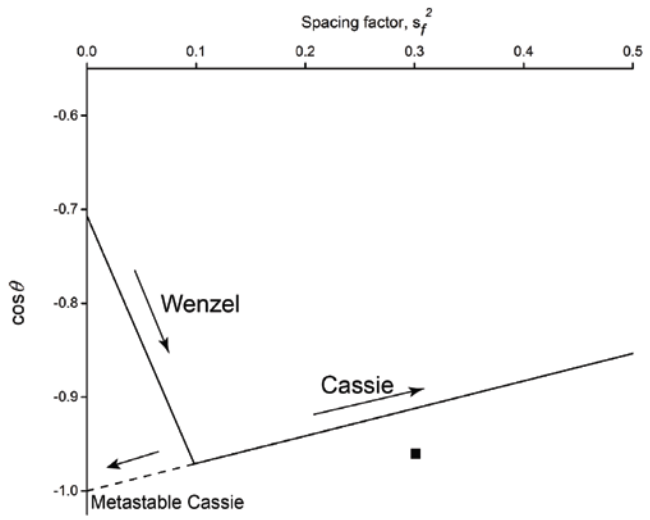

Figure 6 Transition between the Wenzel and Cassie–Baxter regimes on the one-tier sample for the advancing case ($\boldsymbol{\theta_{0,adv} = 135°}$). The advancing transition occurs at $\boldsymbol{s_f^2 = 0.098}$.

The position of the black square is determined by both the spacing factor s_f and the experimentally measured dynamic advancing contact angle on the one-tier surface. Owing to the propinquity of the Cassie line and our experimental value, the advancing motion on the one-tier sample can be considered in the Cassie–Baxter mode. We only observed a slight change (~ 2° to 4°) in the dynamic advancing contact angle on the one-tier surface during the droplet transport. Hence, on the advancing frontier, the liquid (and the contact line) stays on top of the micropillars and the Cassie–Baxter motion results in

a smaller advancing contact line friction coefficient. According to the above analysis, the Cassie–Baxter behavior is highly expected for the advancing contact line movement when $s_f^2 > 0.098$.

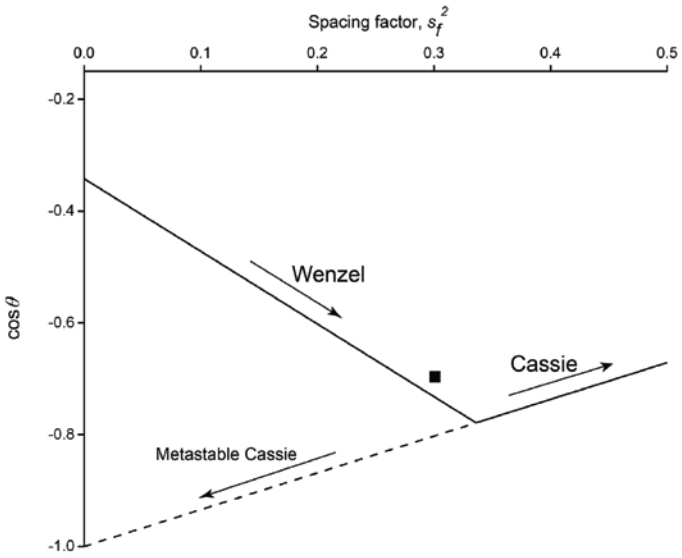

Figure 7 Transition between the Wenzel and Cassie–Baxter regimes on the one-tier sample for the receding case ($\boldsymbol{\theta_{0,rec} = 110°}$). The receding transition occurs at $\boldsymbol{s_f^2 = 0.34}$.

Figure 7 illustrates the transition between the Wenzel and Cassie regimes in the receding transport of a water droplet on the one-tier surface ($\theta_{0,rec} = 110°$). The Wenzel-Cassie transition occurs at $s_f^2 = 0.34$ whereas the one-tier sample has $s_f^2 = 0.3$. The black square in Figure 7 indicates our experimental value in the receding case. The position of the black square is determined by both the spacing factor s_f and the measured receding contact angle on the one-tier surface. Due to the propinquity of the Wenzel state line and our experimental value, the receding motion on the one-tier sample is considered in the Wenzel mode (since $s_f^2 < 0.34$). Wenzel droplets are characterized by large contact angle hysteresis and sticky behaviors. Indeed, our experiments show that the receding contact line behavior on the one-tier sample is highly sticky and a relatively large contact angle hysteresis in the range of 30°-50° was observed. According to Figures 6 and 7, the Cassie state to Wenzel state transition would occur by decreasing s_f^2, which means that increasing the pitch size while reducing the width of the square pillars can transform a Cassie droplet to a Wenzel droplet. As can be seen in these figures, the transition from the Cassie state to the Wenzel state in the advancing case occurs at a lower value of s_f^2 than in the receding case. The corresponding values of s_f^2 for the advancing and receding Cassie-Wenzel transitions are 0.098 and 0.34, respectively, which indicates that Cassie state is the more favorable mode in the advancing event. The receding motion follows the Wenzel mode up to a higher value of $s_f^2 = 0.34$. As a result, on micropillars with $0.098 < s_f^2 < 0.34$, the receding motion still remains sticky. Figure 8 illustrates the dynamic behavior of the advancing and receding contact lines on the one-tier surface with $0.098 < s_f^2 < 0.34$.

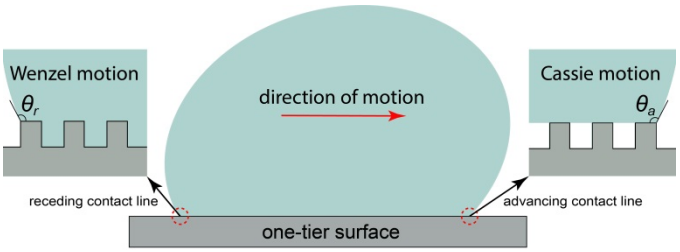

Figure 8 Dynamic behavior of the advancing and receding contact lines on the one-tier surface with $\boldsymbol{0.098 < s_f^2 < 0.34}$.

In this interval, the advancing contact line stays in the Cassie state while the receding contact line follows the Wenzel behavior. The receding motion follows the Wenzel model with droplet filling up the cavities between the micropillars in the vicinity of the receding contact line. Therefore, in the receding case the droplet is in contact with not only the top of the micropillars but also the surfaces between the micropillars In contrast, advancing contact line stays on top of micropillars.

In order to study the wettability of the two-tier surface, we derived the corresponding relations of r and f for this multiscale surface. As can be seen in Figure 1, the two-tier structure consists of multiple roughnesses, i.e., cylindrical nanopillars on the square micropillars. For the case that we have only nanopillars, we have:

$$r_n = 1 + \frac{\pi D_n h_n}{p_n^2} \tag{11}$$

$$f_n = \frac{\pi D_n^2}{4 p_n^2} \tag{12}$$

where D_n is the diameter, p_n is the pitch, and h_n is the height of the cylindrical nanopillars. Taking the roughness of the micropillars (first tier) into account, the roughness factor r and solid-liquid contact fraction f on the two-tier surfaces can be estimated as:

$$r = r_m . r_n \ , \ f = f_m . f_n \tag{13}$$

Therefore, the Wenzel and Cassie–Baxter relations (eqs 2 and 3) on the two-tier surface can be given by:

Wenzel: $$\cos\theta_W = (1+\frac{4a_m h_m}{p_m^2})(1+\frac{\pi D_n h_n}{p_n^2})\cos\theta_0 \quad (14)$$

Cassie–Baxter: $$\cos\theta_{CB} = \frac{a_m^2}{p_m^2}(\frac{\pi D_n^2}{4p_n^2})(\cos\theta_0 + 1) - 1 \quad (15)$$

By substituting the geometric variables of the two-tier sample into the above relations, we have the following relations:

Wenzel: $$\cos\theta_W = 6.5\cos\theta_0 \quad (16)$$

Cassie–Baxter: $$\cos\theta_{CB} = 0.06(\cos\theta_0 + 1) - 1 \quad (17)$$

The following table compares the values of *r* and *f* for one-tier and two-tier surfaces:

Table 1 Comparison of the Wenzel and Cassie–Baxter equations on the one-tier and two-tier structures

Surface	Wenzel model	Cassie–Baxter model
one-tier	$\cos\theta_w = 2.17\cos\theta_y$	$\cos\theta_{CB} = 0.3(\cos\theta_y + 1) - 1$
two-tier	$\cos\theta_w = 6.5\cos\theta_y$	$\cos\theta_{CB} = 0.06(\cos\theta_y + 1) - 1$

The surface roughness of the two-tier structure is significantly higher than that of the one-tier structure. Increasing the roughness of a hydrophobic surface vastly improves its hydrophobicity. By raising the roughness factor, air can be easily trapped underneath the water droplet. The above table shows that the solid-liquid contact fraction *f* on the two-tier surface is 5 times smaller than that of the one-tier surface. This fact reveals that the wetted solid surface underneath the water droplet on the two-tier surface is substantially smaller than that of the one-tier surface. Therefore, the contact angle hysteresis and friction coefficient are extremely low on the two-tier structure. Hence, it was the Cassie–Baxter model that dominated the droplet transport (both advancing and receding) on the two-tier surface.

CONTACT ANGLE HYSTERESIS

Contact angle hysteresis (CAH) is an important factor in determining the wetting properties of a surface [22,23]. Dynamic CAH is by definition the difference between the dynamic advancing and dynamic receding contact angles at a specific velocity of a liquid droplet. As droplet movement is impeded by CAH on a surface, a smaller dynamic CAH results in a lower contact line friction coefficient (i.e., an easier motion). Figure 9 compares the dynamic CAH versus the stage velocity on different surfaces for a water droplet of 15 μl. This figure shows the pronounced effect of surface roughness on dynamic CAH. According to our measurements, the smooth surface exhibits dynamic CAH in the range of 9° to 26°. Dynamic CAH on the one-tier surface (with micropillars) has the highest value (30° to 50°).

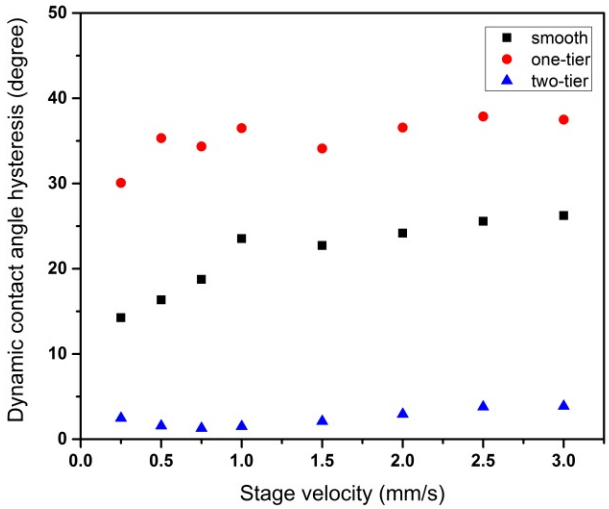

Figure 9 Comparison of the dynamic contact angle hysteresis on different surfaces.

As discussed before, the markedly large CAH on the one-tier sample is mainly due to the Wenzel behavior of the receding contact line. The integration of micro- and nano-structures on the two-tier superhydrophobic surface can make the droplet advancing and receding transport both in the Cassie mode that gives rise to an extremely low dynamic CAH of 1° to 4°. Figure 10 summarizes our experimental results on smooth, one-tier, and two-tier surfaces.

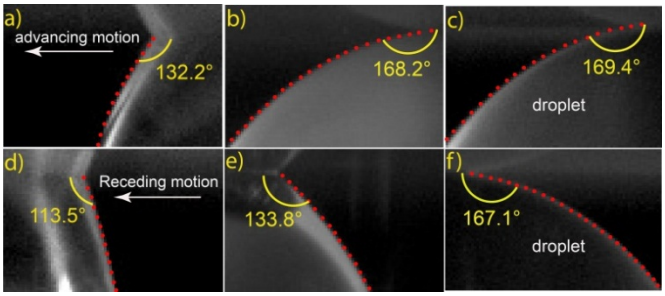

Figure 10 a, b, c) Advancing contact angles on a) smooth, b) one-tier and c) two-tier surfaces, d, e, f) Receding contact angles on d) smooth, e) one-tier, and f) two-tier surfaces. The static contact angles are equal to123.0° on a smooth surface, 166.2° on a one-tier surface, and 167.8° on a two-tier surface. The corresponding dynamic CAHs are 18.7° on a smooth surface, 34.4° on a one-tier surface, and 2.3° on a two-tier surface. The droplet volume in all cases is 15μl and the bottom stage velocity is 0.75 mm/s. All samples are coated with a thin layer of fluoropolymer.

The two-tier surface has the lowest dynamic CAH (i.e., the easiest motion) and the one-tier surface presents the highest dynamic CAH due to receding contact line pinning.

CONCLUSION

In this work we investigated the effects of surface roughness on dynamic behavior of water droplets on different types of hydrophobic surfaces. Advancing and receding contact line friction coefficients were measured, analyzed and compared on smooth, one-tier (with micropillars), and two-tier (with CNTs on micropillars) surfaces over a wide range of contact line velocities and droplet volumes. Advancing and receding contact line friction coefficients on these surfaces were found to follow the following relations:

advancing: $\xi_{smooth} > \xi_{one-tier} > \xi_{two-tier}$

while

receding: $\xi_{one-tier} > \xi_{smooth} > \xi_{two-tier}$

Our measurements indicate that two-tier superhydrophobic surfaces with multiscale micro\nano-structures can remarkably facilitate liquid movement and have the lowest advancing and receding contact line friction coefficients. The advancing and receding contact line friction coefficients on the smooth surface are >10 times larger than those on the two-tier surface. However, the receding contact line friction coefficient on the one-tier sample was found to be significantly larger than the advancing coefficient. In order to fully understand the dynamic behaviors of the advancing and receding transports on the one-tier surface, a comprehensive analysis was carried out on the Wenzel-Cassie transition. According to our experiments, the receding motion on the one-tier surface was in the Wenzel mode (highly sticky) leading to the significant CAH on the one-tier surface. However, the slippery behavior of the advancing contact line was attributed to the Cassie state. Furthermore, our experimental work demonstrates that the multiscale textured surfaces can substantially reduce the advancing and receding frictions by keeping both the advancing and receding contact lines in the Cassie-Baxter mode. Indeed, multiscale roughness on the two-tier surface greatly facilitates the droplet transport with less friction.

REFERENCES

[1] Neinhuis, C.; Barthlott, W., Characterization and distribution of water-repellent, self-cleaning plant surfaces. *Annals of Botany* **1997,** *79* (6), 667-677.

[2] Barthlott, W.; Neinhuis, C., Purity of the sacred lotus, or escape from contamination in biological surfaces. *Planta* **1997,** *202* (1), 1-8.

[3] Wagner, P.; Fürstner, R.; Barthlott, W.; Neinhuis, C., Quantitative assessment to the structural basis of water repellency in natural and technical surfaces. *Journal of Experimental Botany* **2003,** *54* (385), 1295-1303.

[4] Bhushan, B.; Jung, Y. C., Micro-and nanoscale characterization of hydrophobic and hydrophilic leaf surfaces. *Nanotechnology* **2006,** *17* (11), 2758.

[5] Patankar, N. A., Mimicking the lotus effect: influence of double roughness structures and slender pillars. *Langmuir* **2004,** *20* (19), 8209-8213.

[6] Sun, M.; Luo, C.; Xu, L.; Ji, H.; Ouyang, Q.; Yu, D.; Chen, Y., Artificial lotus leaf by nanocasting. *Langmuir* **2005,** *21* (19), 8978-8981.

[7] Jeong, W.-J.; Ha, M. Y.; Yoon, H. S.; Ambrosia, M., Dynamic Behavior of Water Droplets on Solid Surfaces with Pillar-Type Nanostructures. *Langmuir* **2012,** *28* (12), 5360-5371.

[8] Dorrer, C.; Rühe, J., Advancing and receding motion of droplets on ultrahydrophobic post surfaces. *Langmuir* **2006,** *22* (18), 7652-7657.

[9] Cheng, J.-T.; Vandadi, A.; Chen, C.-L., Condensation heat transfer on two-tier superhydrophobic surfaces. *Applied Physics Letters* **2012,** *101* (13), 131909-131909-4.

[10] Jung, Y.; Bhushan, B., Wetting behaviour during evaporation and condensation of water microdroplets on superhydrophobic patterned surfaces. *Journal of microscopy* **2008,** *229* (1), 127-140.

[11] Voué, M.; Rioboo, R.; Adao, M.; Conti, J.; Bondar, A.; Ivanov, D.; Blake, T.; De Coninck, J., Contact-line friction of liquid drops on self-assembled monolayers: chain-length effects. Langmuir 2007, 23 (9), 4695-4699.

[12] Lee, D.-G.; Park, J.; Bae, J.; Kim, H.-Y., Dynamics of a microliquid prism actuated by electrowetting. *Lab on a Chip* **2013,** *13* (2), 274-279.

[13] Blake, T. D.; Clarke, A.; Stattersfield, E., An investigation of electrostatic assist in dynamic wetting. *Langmuir* **2000,** *16* (6), 2928-2935.

[14] De Ruijter, M. J.; Blake, T.; De Coninck, J., Dynamic wetting studied by molecular modeling simulations of droplet spreading. *Langmuir* **1999,** *15* (22), 7836-7847.

[15] Nakajima, A.; Hashimoto, K.; Watanabe, T., Recent studies on super-hydrophobic films. *Monatshefte für Chemie/Chemical Monthly* **2001,** *132* (1), 31-41.

[16] Zhai, L.; Cebeci, F. C.; Cohen, R. E.; Rubner, M. F., Stable superhydrophobic coatings from polyelectrolyte multilayers. *Nano Letters* **2004,** *4* (7), 1349-1353.

[17] Wenzel, R. N., Resistance of solid surfaces to wetting by water. *Industrial & Engineering Chemistry* **1936,** *28* (8), 988-994.

[18] Cassie, A.; Baxter, S., Wettability of porous surfaces. *Transactions of the Faraday Society* **1944,** *40*, 546-551.

[19] McHale, G.; Shirtcliffe, N.; Newton, M., Contact-angle hysteresis on super-hydrophobic surfaces. *Langmuir* **2004,** *20* (23), 10146-10149.

[20] Quéré, D.; Lafuma, A.; Bico, J., Slippy and sticky microtextured solids. *Nanotechnology* **2003,** *14* (10), 1109.

[21] Nosonovsky, M.; Bhushan, B., Biomimetic superhydrophobic surfaces: multiscale approach. *Nano letters* **2007,** *7* (9), 2633-2637.

[22] Bonn, D.; Eggers, J.; Indekeu, J.; Meunier, J.; Rolley, E., Wetting and spreading. *Reviews of modern physics* **2009,** *81* (2), 739.

[23] Extrand, C., Contact angles and hysteresis on surfaces with chemically heterogeneous islands. *Langmuir* **2003,** *19* (9), 3793-3796.